APPENDIX

A. THE DATA

The utilized photometric bands for W-CDF-S are VOICE *ugri* (Vaccari et al. 2016), HSC *griz* (Ni et al. 2019), VIDEO $ZYJHK_s$ (Jarvis et al. 2013), and DeepDrill 3.6 and 4.5 μm (Lacy et al. 2021); the bands for ELAIS-S1 are VOICE *u*, DES DR2 *grizY* (Abbott et al. 2021), ESIS *BVR* (Berta et al. 2006; Vaccari et al. 2016), VIDEO $ZYJHK_s$, and DeepDrill 3.6 and 4.5 μm. The photometric data are corrected for Galactic extinction following the method in Section 5.5 of Yang et al. (2014); see also https://irsa.ipac.caltech.edu/applications/DUST/. The compilation of spec-*z*s is described in Ni et al. (in preparation), and interested readers can refer to their article for more details.

Our cataloged sources are required to be detected in VIDEO. However, the VIDEO survey in the 4.9 deg^2 W-CDF-S field is not uniform, and some regions are shallower than ELAIS-S1 or even are not covered in some bands; e.g., the *Z* band only covers 1.8 deg^2 of the entire W-CDF-S field. Therefore, W-CDF-S has a slightly smaller surface number density on deg^2 scales than ELAIS-S1.

B. THE DEPTH OF HIGH-QUALITY PHOTO-*Z*S

To assess quantitatively how the fraction of high-quality photo-*z*s drops as a function of *i*-band magnitude ($i_{\rm mag}$), we fit our data with the following formulae:

$$p(i_{\rm mag}) = \frac{a_1}{1+\exp\left[a_2(i_{\rm mag}-a_3)\right]} + a_4, \tag{B1}$$

$$\delta_{Q_z<1} \sim Bernoulli(p), \tag{B2}$$

where (a_1, a_2, a_3, a_4) are parameters to be fitted, $p(i_{\rm mag})$ is the probability that a source with $i_{\rm mag}$ has $Q_z < 1$, and $\delta_{Q_z<1}$ is defined as 1 if $Q_z < 1$ and 0 if $Q_z \geq 1$. a_3 can be regarded as a nominal magnitude, below which $p(i_{\rm mag})$ drops considerably (if $a_2 > 0$). By maximizing the corresponding likelihoods, we obtain

$$p(i_{\rm mag}) = \frac{0.37}{1+\exp\left[2.56(i_{\rm mag}-23.9)\right]} + 0.50 \text{ for W-CDF-S with SNR cuts,} \tag{B3}$$

$$p(i_{\rm mag}) = \frac{0.63}{1+\exp\left[1.87(i_{\rm mag}-24.3)\right]} + 0.23 \text{ for W-CDF-S without SNR cuts,} \tag{B4}$$

$$p(i_{\rm mag}) = \frac{0.48}{1+\exp\left[2.91(i_{\rm mag}-23.8)\right]} + 0.42 \text{ for ELAIS-S1 with SNR cuts,} \tag{B5}$$

$$p(i_{\rm mag}) = \frac{0.79}{1+\exp\left[2.38(i_{\rm mag}-24.1)\right]} + 0.10 \text{ for ELAIS-S1 without SNR cuts,} \tag{B6}$$

where "SNR cuts" means that we only select sources having SNR > 5 detections in more than 5 bands.

Fig. S1 justifies that these functions can generally match well the observed fraction of high-quality photo-*z*s as a function of $i_{\rm mag}$. The figure also shows that applying the SNR cut can greatly improve the overall photo-*z* quality in the faint-magnitude regime. The best-fit a_3 values are generally around 24, and thus we conclude that the nominal *i*-band "depths" of our high-quality photo-*z*s are ~ 24 for both W-CDF-S and ELAIS-S1. The $p(i_{\rm mag})$ values of ELAIS-S1 can generally match those of W-CDF-S at $i_{\rm mag} \lesssim 24$. At fainter magnitudes, the ELAIS-S1 $p(i_{\rm mag})$ drops to a lower level than the W-CDF-S $p(i_{\rm mag})$ because the *griz* data in ELAIS-S1 are shallower.

C. ADDITIONAL NOTES ON FIGURE 1

There are a few sources that have non-zero spec-*z*s but have near-zero photo-*z*s. This phenomenon may arise because the `EAZY` code cannot find an obvious Balmer break at 3646 Å for these sources when no bands cover the break, and thus it assigns the photo-*z*s to be ~ 0.

D. NOTES ON THE PHOTO-*Z* UNCERTAINTIES

The cataloged photo-*z* is the *z*-grid value that minimizes the fitting χ^2 output by `EAZY`, and the 68% limits are the redshift values of the photo-*z* quantile function from the fitting at 16% and 84% (see Eq. 6 of Brammer et al. 2008). The definition of the best-fit

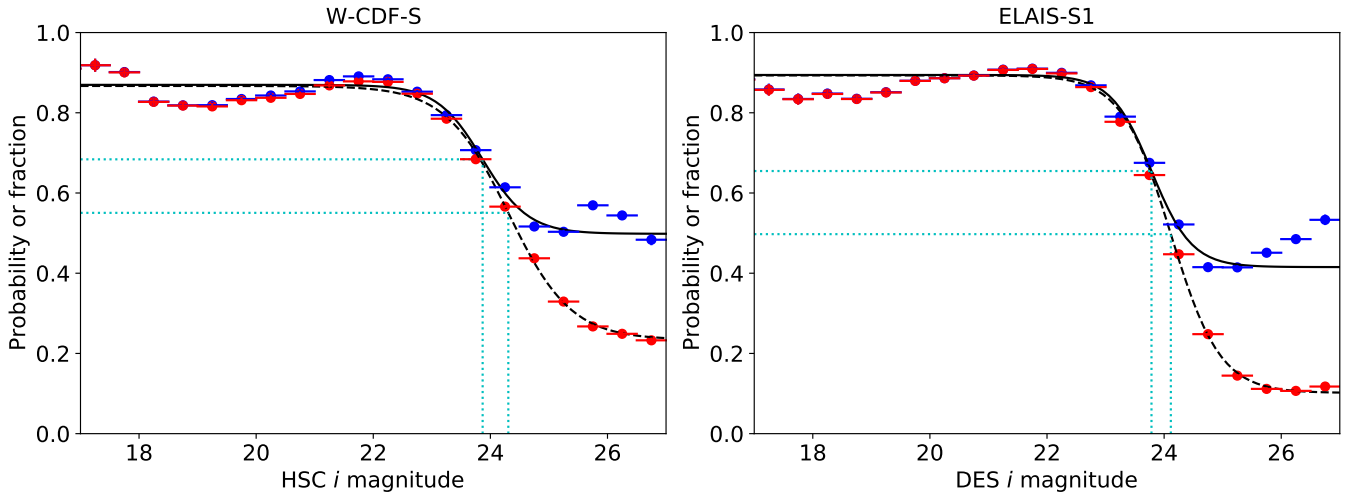

Figure S1. The points with error bars are the fractions of high-quality photo-zs in magnitude bins with widths = 0.5 mag for W-CDF-S (*left*) and ELAIS-S1 (*right*). The blue and red points represent cases with and without SNR cuts, respectively. The black curves are the best-fit probabilities, $p(i_{\rm mag})$, of obtaining a high-quality photo-z for a source as a function of its i-band magnitude. The solid and dashed curves are for cases with and without SNR cuts, respectively. The cyan dotted lines mark the nominal depths (i.e., a_3) of our high-quality photo-zs as well as the corresponding $p(i_{\rm mag})$ values. The points and curves are generally consistent.

photo-z does not require it to be necessarily within the photo-z uncertainty interval; thus, there are a small fraction of sources with photo-zs smaller/larger than their 68% lower/upper limits, and the limits of these sources should not be used (Yang et al. 2014). Furthermore, we found that 78%/76% of spec-zs reside within the 68% photo-z intervals in W-CDF-S/ELAIS-S1. This may indicate that the photo-z uncertainties are slightly overestimated (i.e., 78%/76% roughly correspond to 1.2 σ for a normal distribution).

E. NOTES ON AGNS AND STARS

As mentioned in the main text, we only use galaxy templates to fit all the sources, and thus the results may be less reliable for AGNs and stars. For AGNs, however, only those that materially affect the observed optical-to-near-infrared (NIR) SEDs are expected to have this issue, and such sources are usually BL AGNs. Other sources with at most moderate AGN contributions to the optical-to-NIR SEDs (e.g., obscured AGNs) generally still have reliable photo-zs. For example, Ni et al. (in preparation) show that $f_{\rm outlier}$ in W-CDF-S/ELAIS-S1 are 6.8%/4.4% for non-BL X-ray AGNs with high-quality photo-zs. Therefore, for most work involving AGNs in W-CDF-S and ELAIS-S1, to obtain optimal photo-zs, it is usually sufficient to divide their sample to BL AGNs and other sources and adopt the photo-zs in Ni et al. (in preparation) for the former and our photo-zs for the latter. We emphasize that the term "BL AGNs" here does not only refer to those AGNs with spectroscopically detected broad lines, but is generalized to mean all the sources with significant characteristics that are similar to spectroscopic BL AGNs, such as those sources with AGN-dominated SEDs.

In addition, BL AGNs are not expected to be dominant among the outliers in Fig. 1 because BL AGNs have a much lower surface number density ($\lesssim 300$ deg^{-2}; Ni et al., in preparation) than galaxies. Only 5%/16% of the outliers in W-CDF-S/ELAIS-S1 are identified as BL AGN candidates (Ni et al., in preparation), and these values further drop to 3%/5% when requiring $Q_z < 1$.

Detailed selections of BL AGNs and stars are beyond the scope of this work. Thus, we leave the selections to the users of this catalog who can apply their own criteria, and they can also adopt the selections in Ni et al. (in preparation) for both BL AGNs and stars.

REFERENCES

Abbott, T. M. C., Adamow, M., Aguena, M., et al. 2021, arXiv e-prints, arXiv:2101.05765. https://arxiv.org/abs/2101.05765

Berta, S., Rubele, S., Franceschini, A., et al. 2006, A&A, 451, 881, doi: 10.1051/0004-6361:20054548

Brammer, G. B., van Dokkum, P. G., & Coppi, P. 2008, ApJ, 686, 1503, doi: 10.1086/591786

Jarvis, M. J., Bonfield, D. G., Bruce, V. A., et al. 2013, MNRAS, 428, 1281, doi: 10.1093/mnras/sts118

Lacy, M., Surace, J. A., Farrah, D., et al. 2021, MNRAS, 501, 892, doi: 10.1093/mnras/staa3714

Ni, Q., Timlin, J., Brandt, W. N., & Yang, G. 2019, Research Notes of the American Astronomical Society, 3, 5, doi: 10.3847/2515-5172/aaf8af

Vaccari, M., Covone, G., Radovich, M., et al. 2016, in The 4th Annual Conference on High Energy Astrophysics in Southern Africa (HEASA 2016), 26. https://arxiv.org/abs/1704.01495

Yang, G., Xue, Y. Q., Luo, B., et al. 2014, ApJS, 215, 27, doi: 10.1088/0067-0049/215/2/27